Hypoxia-mediated regulation of DDX5 through decreased chromatin accessibility and post-translational targeting restricts R-loop accumulation

Katarzyna B. Leszczynska[1,2,$], Monika Dzwigonska[2], Hala Estephan[1], Jutta Moehlenbrink[1], Elizabeth Bowler[1], Amato J. Giaccia[1], Jakub Mieczkowski[3], Bozena Kaminska[2] and Ester M. Hammond[1$]

[1]Oxford Institute for Radiation Oncology, Department of Oncology, The University of Oxford, Oxford, OX3 7DQ, UK

[2]Laboratory of Molecular Neurobiology, Neurobiology Center, Nencki Institute of Experimental Biology, Polish Academy of Sciences, Warsaw, Poland.

[3]3P-Medicine Laboratory, Medical University of Gdansk, Gdansk, Poland

[$]corresponding authors

Ester.Hammond@oncology.ox.ac.uk

k.leszczynska@nencki.edu.pl

ORCIDs

EMH - 0000-0002-2335-3146

KBL - 0000-0002-3504-1553

MD - 0000-0003-1774-3671

HE - 0000-0001-7017-0038

JM - 0000-0002-2091-012X

BK - 0000-0002-2642-4616

KEYWORDS: Hypoxia, ATACseq, DDX5, R-loops, TRIM5

ABSTRACT

Local hypoxia (low oxygen) occurs in most solid tumors and is associated with aggressive disease and therapy resistance. Widespread changes in gene expression play a critical role in the biological response to hypoxia. However, most of the prior research has focused on hypoxia-inducible genes in hypoxia as opposed to those which are decreased. Using ATACseq, we demonstrate that chromatin accessibility is decreased in an oxygen-dependent manner, predominantly at gene promoters and specific pathways are impacted including DNA repair, splicing and the R-loop interactome. As R-loops accumulate in hypoxic conditions we hypothesized that an underlying mechanism could be the repression of the R-loop interactome. One of the genes with decreased chromatin accessibility in hypoxia was *DDX5*, encoding the RNA helicase, DDX5, which showed reduced expression in various cancer cell lines in hypoxic conditions, tumor xenografts and in patient samples with hypoxic tumors. In addition, we identified TRIM5 as a novel hypoxia inducible E3 ligase which targets DDX5 for proteasomal degradation independently of changes at mRNA levels. We demonstrate multiple mechanisms contributing to reduced DDX5 expression in hypoxic conditions. Most interestingly, we found that when DDX5 is rescued in hypoxia, R-loop levels accumulate further, therefore demonstrating that hypoxia-mediated repression of DDX5 restricts R-loop accumulation. Together these data support the hypothesis that a critical part of the biological response to hypoxia is the repression of multiple R-loop processing factors, however, as shown for DDX5, their role is specific and distinct.

INTRODUCTION

Oxygen is an essential molecule in most biochemical reactions [1]. During the lifetime of a cell, the oxygen concentration can fluctuate and therefore complex mechanisms have evolved to enable the cell to adapt and survive. Hypoxia is associated with pathological conditions such as cancer, stroke and cardiovascular disease and can lead to cellular and organ damage [2]. In cancer, regions of hypoxia arise when the poorly formed tumour vasculature fails to deliver sufficient oxygen to meet the high metabolic demand of rapidly proliferating cancer cells [3]. The biological response to hypoxia involves a complex transcriptional program including the transactivation of hundreds of genes by the hypoxia inducible factors (HIFs) but also the repression of specific processes, for example the DNA repair pathways [4]. Widespread repression of gene expression in hypoxia has been attributed to attempts to save cellular energy. However, it is also plausible that in specific cases genes/pathways could be actively repressed as a critical part of the biological response to hypoxia.

R-loops are three-stranded nucleic acid structures consisting of an RNA/DNA hybrid and a displaced single-stranded DNA, which originate during transcription [5,6]. We recently demonstrated that R-loop levels increase in response to hypoxia (<0.1% O_2) and that the RNA/DNA helicase, Senataxin (SETX), is also induced in these conditions [7]. An underlying mechanism for the hypoxia-mediated accumulation of R-loops has not been elucidated and the impact at specific gene loci has not been described. Interestingly, while the SETX helicase was induced in hypoxia, the expression of a number of other R-loop-associated factors (R-loop interactome) was decreased, suggesting that the loss of these factors could contribute to the overall increase in R-loop levels [7]. This finding led us to consider that an important biological response to hypoxia is to reduce the expression of R-loop related factors, however, the mechanism of a global decrease of these factors in hypoxia remained unclear.

We and others had shown that hypoxia leads to widespread epigenetic changes, including an increase in repressive histone methylation marks, for example H3K9me3, which is most likely attributed to impaired function of the oxygen-dependent histone lysine demethylases (KDM) [8–10]. Here, we investigated whether epigenetic changes affecting chromatin accessibility could contribute to the loss of the R-loop interactome in hypoxic conditions. As both the DNA repair and splicing pathways are repressed in hypoxic conditions and linked to R-loop formation and resolution, we assessed if changes in chromatin accessibility might be responsible for the loss of these pathways [4,11]. Using the assay for transposase-accessible chromatin with sequencing (ATAC-seq) we found a decrease in chromatin accessibility at the promoters of a number of genes encoding RNA processing factors, including R-loop-associated helicases. We focused on DDX5 which is an ATP-dependent DEAD/H-box RNA helicase, with diverse roles in mRNA splicing, co-activation of transcription factors, nonsense mediated decay and resolving R-loops [12–19]. Here, we demonstrate the repression of DDX5 at the transcriptional and post-translational levels in hypoxia and identify TRIM5 as an E3 ligase which targets DDX5 for proteasomal degradation. We show that restoring DDX5 levels in hypoxia results in further accumulation of R-loops, suggesting that the repression of DDX5 in hypoxia restricts R-loop accumulation.

RESULTS

To investigate the potential role of epigenetic changes in the regulation of the R-loop interactome in hypoxia we employed a murine glioblastoma model, GL261, which is known to develop hypoxic areas when grown orthotopically (**Supplementary Figure 1A**) [20]. Firstly, we assessed the changes in chromatin marks associated with a repressive heterochromatin state in hypoxia. GL261 cells were exposed to either moderate (1% O_2) or severe (<0.1% O_2) hypoxia

and changes in chromatin marks were determined. As expected, we observed a marked increase in H3K9 and H3K27 trimethylation [8,9,21] (**Figure 1A**). However, we also observed an increase in H3K4 trimethylation, which is an activating histone modification. In all cases, increased methylation was most pronounced in the more severe hypoxia (<0.1% O_2) and was reduced to near normoxic levels as quickly as 1 hour after reoxygenation, further emphasizing oxygen-dependent changes in chromatin (**Figure 1A** and **Supplementary Figure 1B**).

Since hypoxia-increased methylation marks could have a repressive or activating influence on gene expression, we investigated the landscape of chromatin accessibility in cells in hypoxic conditions. We carried out ATACseq analysis on GL261 cells exposed to hypoxic (1 or <0.1% O_2) or normoxic (21% O_2) conditions. To prevent any reoxygenation-dependent changes in the chromatin that could occur during processing of samples, we employed a modification of ATACseq that allows fixation of cells prior to lysis [22]. Principal component analysis (PCA) showed a significant separation of ATACseq profiles between normoxic and the two hypoxic conditions (**Figure 1B**). Overall, we detected 41,733 ATACseq peaks, of which 67.3% were detected in all conditions, 2.25% were specific to normoxia, 8.23% were specific to 1% O_2 and 6.6% were specific to <0.1% O_2 conditions (**Figure 1C)**. We then carried out a differential peak analysis between hypoxic and normoxic conditions and identified a total of 5,920 peaks with differential chromatin accessibility at 1% O_2 and 9,792 peaks with differential chromatin accessibility at <0.1% O_2, both significantly altered in relation to the normoxic control (**Figure 1D-E**). Of these, 3,091 peaks were significantly increased, and 2,829 peaks were significantly decreased at 1% O_2, while 4,948 peaks were significantly increased, and 4,844 peaks were significantly decreased at <0.1% O_2 (**Figure 1D-E** and **Supplementary Table 1**). Overall, severe hypoxia led to a greater number of significant ATACseq peak changes, which reflects the oxygen-dependent changes in histone methylation that are known to contribute to the chromatin accessibility (**Figure 1A** and **Supplementary Figure 1B)** [23,24]. Next, we carried out

genomic annotation of the differentially regulated ATACseq peaks in hypoxia (1 and <0.1% O_2) (**Figure 1F**). One of the most notable differences between the response to moderate (1% O_2) and severe (<0.1% O_2) hypoxia was the number of ATACseq peaks lost at promoter regions, with nearly 1000 peaks lost in 1% O_2 and over 3000 peaks lost in <0.1% O_2. (**Figure 1F**). The oxygen dependency was further emphasized when a ratio between a percentage of decreased peaks at specific genomic annotations in severe versus moderate hypoxia was evaluated (**Supplementary Figure 2A-C**), where again the highest percentage of decreased ATACseq peaks at promoter regions was in response to severe hypoxia compared to moderate hypoxia (**Supplementary Figure 2C** and **Supplementary Table 2**). Moreover, the majority of repressed promoter peaks identified in moderate hypoxia (789 out of 852) were included in the peaks repressed in severe hypoxia (**Supplementary Figure 2D**). However, severe hypoxia repressed additional promoters, demonstrating the oxygen dependency of this process. Since severe hypoxia induced the greatest loss of accessible promoters, we performed a functional enrichment analysis of the genes with significantly decreased ATACseq peaks at promoter regions in severe hypoxia using three databases: Gene Ontology (GO), Kyoto Encyclopedia of Genes and Genomes (KEGG) and Reactome [25–27]. We identified a number of signaling pathways associated with the peaks decreased in severe hypoxia, many of which were related to RNA metabolism and processing, including ribonucleotide complex biogenesis, ncRNA metabolic process or mRNA processing and splicing. The top ten significantly downregulated pathways from GO analysis based on the highest gene count associated with each pathway are shown (**Figure 1G,** full list of significantly associated pathways **Supplementary Table 3**).

In order to validate the results of our ATACseq analysis, we focused on genes involved in splicing, as components of this pathway have previously been shown to be transcriptionally repressed in hypoxia [11]. From the list of the spliceosome genes, we identified a number of splicing factors as having decreased ATACseq peaks in hypoxia (**Supplementary Table 4**)

and confirmed that 10 of them were repressed at the mRNA level (**Figure 1H, I**). This was in contrast to the mRNA of known HIF targets, *Slc2a1* or *Vegfa*, which are induced in response to hypoxia [28]. Moreover, the functional analyses of decreased ATACseq peaks in gene promoter regions led to the identification of other pathways, including the DNA repair pathways such as base excision repair, homology-directed repair, double strand break repair and non-homologous end-joining (Reactome analysis, **Supplementary Table 3**) [4]. Overall, our data identifies a global mechanism of hypoxia-induced repression of multiple pathways linking previously reported mRNA repression with decreased chromatin accessibility.

Loss of chromatin accessibility at the promoters of genes coding for RNA-processing factors supports our hypothesis that the repression of genes involved in R-loops could be mediated by epigenetic changes, as many of these genes have been identified in the R-loop interactome. The RNA or RNA/DNA helicases *Ddx1, Ddx3x, Ddx5, Ddx18, Ddx21, Ddx27, Ddx39b, Dhx9, Dhx15, Srsf1, Xrn2* and *Prkdc* are all components of the R-loop interactome and were all found to have reduced chromatin accessibility in their promoters in hypoxia (**Figure 2A, Supplementary Table 5**) [29]. Of these helicases, we have shown previously that *DHX9* mRNA expression is repressed in hypoxia (<0.1% O_2) therefore supporting a link between these ATACseq data and gene expression in hypoxia (**Figure 2B**) [7]. In contrast, chromatin accessibility did not change at the *SETX* gene promoter (**Supplementary Figure 2E**), consistent with the recently identified increase in *SETX* expression in response to hypoxia (<0.1% O_2) [7].

Next, we asked if changes in chromatin accessibility correlated with changes in protein expression levels. We investigated the levels of the DHX9 and DDX5 helicases and found that DHX9 and DDX5 protein levels were significantly decreased in cells exposed to hypoxia (<0.1% O_2). In both cases, this decrease was quickly reversed when oxygen was restored to normoxic levels (**Figure 2C**).

DDX5 expression has not previously been linked to the response to tumor hypoxia and therefore, we investigated expression in a panel of human cell lines. In all of the tested cancer cell lines, including lung, esophageal, colorectal, bladder, bone and glioma cells, DDX5 protein was repressed in response to hypoxia (<0.1% O_2) (**Figure 2D-G** and **Supplementary Figure 3A-D**). Notably, a similar change occurred in non-cancer MRC-5 cells, indicating that the hypoxia-mediated repression of DDX5 is not restricted to cancer cells (**Figure 2G**). To investigate the oxygen-dependency of DDX5 repression and possible HIF involvement, we exposed cells to a range of hypoxic conditions (<0.1 or 2% O_2) as well as the hypoxia mimetics $CoCl_2$ and DFO. DDX5 levels decreased in response to 2% O_2, although less than observed after exposure to <0.1% O_2 (**Figure 2H)**. However, both $CoCl_2$ and DFO, which stabilize HIF-1 in normoxic conditions, had little or no effect on DDX5 expression, indicating that the repression of DDX5 is not dependent on HIF-mediated signaling (**Figure 2H** and **Supplementary Figure 3E**). Finally, we analyzed tumor xenografts (HCT116, OE-21 and GL261) for both hypoxia (using pimonidazole) and DDX5 expression. In all three tumor types, an inverse correlation was observed between hypoxia (pimonidazole positive) and DDX5 expression, confirming that hypoxia represses DDX5 protein expression *in vivo* (**Figure 2 I-K**).

DDX5 is known to interact with its paralog DDX17 and depletion of DDX5 has been shown to upregulate DDX17 [14]. When we depleted DDX5 using siRNA, the levels of DDX17 increased significantly in normoxic conditions confirming the compensatory relationship between DDX17 and DDX5 (**Supplementary Figure 3F-G**). However, in hypoxic conditions, where DDX5 was repressed, the expression of DDX17 did not change indicating that this compensatory relationship does not occur in hypoxia. Together, these data suggest that DDX5 is repressed in an oxygen-dependent manner and this event does not result in increased expression of DDX17.

Our ATACseq data (**Figure 2A-B**) suggests that DDX5 expression is likely controlled at the transcriptional level. To further investigate potential links between DDX5 and hypoxia in cancer, we first determined if *DDX5* mRNA and a validated hypoxia signature are correlated in TCGA cancer patient cohorts (glioblastoma, breast, colorectal, bladder, lung adenocarcinoma and lung squamous cell carcinoma). We found a significant inverse correlation between *DDX5* mRNA and the hypoxic signature in five out of the six tested datasets (**Figure 3A**). These findings suggested that DDX5 mRNA expression is repressed in hypoxic tumors. This association was further verified in cancer cell lines with qPCR. In three of the tested cell lines (HCT116, OE21, FLO1), we observed significant repression of the *DDX5* mRNA (approximately 50% of the normoxic control) in contrast to the HIF-1 target *VEGFA* which was induced in hypoxia (**Figure 3B**). However, *DDX5* mRNA was unchanged in response to hypoxia in RKO cells despite the clear reduction of DDX5 protein (**Figure 2E**, **Figure 3B** and **Supplementary Figure 3E** and **G**). This finding raised the possibility of an additional post-translational mechanism of repression.

We tested the involvement of the proteasome pathway in repression of DDX5 and confirmed that DDX5 protein was degraded via the proteasome in hypoxia by co-treating with MG-132 (**Figure 3C**). We then went on to investigate the half-life of the DDX5 protein in hypoxia and in normoxia and surprisingly, found that blocking global protein translation in hypoxia with cycloheximide prevented DDX5 degradation (**Figure 3D**). Using emetine, as an alternative agent to block translation, we further confirmed that hypoxia-mediated repression of DDX5 could be reversed by blocking translation (**Supplementary Figure 5A**). These data suggest that active translation is required in hypoxic conditions to decrease the levels of DDX5 and led to the hypothesis that an E3 ligase is induced in hypoxia which in turn targets DDX5 for proteasomal degradation (**Figure 3E**).

As an E3 ligase for DDX5 had not been described, we used the UbiBrowser platform and identified the related E3 ligases and viral restriction factors, ZEB2, TRIM5 and TRIM21 as candidate E3 ligases for DDX5 (http://ubibrowser.bio-it.cn/ubibrowser/; version UbiBrowser$^{1.0}$) [30]. To test this hypothesis, we determined the expression of both *TRIM5* and *TRIM21* mRNA in hypoxic conditions. We did not investigate ZEB2 as a candidate, as we have shown previously that ZEB2 expression is repressed in hypoxia [21]. In contrast to *TRIM21*, the levels of *TRIM5* were significantly induced (8-fold) in response to hypoxia, comparable to the levels of the HIF target, *VEGFA* (**Figure 4A**). To explore a potential link between TRIM5 and DDX5, we determined the protein levels of both and found that an increase in TRIM5 expression was concomitant with the loss of DDX5 in hypoxia (**Figure 4B-C**). This reciprocal expression pattern was observed in a number of cancer and non-cancer cell lines, suggesting that TRIM5 could be regulating DDX5 levels (**Figure 4D**). To determine the mechanism of TRIM5 induction in hypoxia, we first investigated the oxygen dependency of this response. While expression of TRIM5 was induced at <0.1% O_2, there was no significant increase of TRIM5 in response to 2% O_2 (**Figure 4E** and **Supplementary Figure 5B-C**). These data suggest that TRIM5 is unlikely to be regulated by the HIF family of transcription factors, which are active at both 2 and <0.1% O_2.

TRIM5 has previously been shown to be responsive to interferons α (IFNα) and β (IFNβ) and transcriptionally induced through STAT1 binding to the interferon-stimulated response element present at the TRIM5 promoter region [31]. We investigated whether hypoxia induces TRIM5 through IFNα and STAT1/3. As expected, we found that both TRIM5 mRNA and protein were increased in response to IFNα (but not IFNγ), which was completely abrogated in the presence of Ruxolitinib, the JAK1/2 inhibitor acting upstream of STAT1 and STAT3 (**Supplementary Figure 5B-C**) [32]. However, hypoxia-dependent induction of TRIM5 remained unchanged in the presence of Ruxolitinib. In addition, we did not observe any

upregulation of phospho-STAT1 (Y701) or phospho-STAT3 (T705) in hypoxic conditions, suggesting that TRIM5 expression is increased in hypoxia independently of IFNα and STAT1/3 signaling. This was consistent with recent reports showing that hypoxia represses the interferon type I response [33]. The oxygen dependency of TRIM5 induction in hypoxia was reminiscent of p53-mediated transcriptional activity and we found that expression of TRIM5 correlated with known p53-induced targets in hypoxia in TCGA cancer patient cohorts (**Supplementary Figure 5D**) [34]. However, TRIM5 was also found to be induced in response to hypoxia in the OE21 cell line which is p53 deficient (**Figure 4F-G**). To clarify a potential role for p53 in hypoxia-mediated induction of TRIM5, we used the genetically matched cell lines HCT116$^{p53+/+}$ and HCT116$^{p53-/-}$ and found that while there was a significant induction of *TRIM5* mRNA in hypoxia in both cell lines, the induction of *TRIM5* mRNA was significantly reduced in hypoxic conditions in p53 deficient cells. In comparison, the validated p53-target, *INPP5D*, was completely abrogated in the HCT116$^{p53-/-}$ cells in both normoxia and hypoxia (**Figure 4H**) [34]. Together, these data demonstrate that TRIM5 is induced in an oxygen-dependent manner through multiple mechanisms, one of which involves p53.

To determine if TRIM5 is the E3 ligase targeting DDX5 via a direct interaction in hypoxia, we immunoprecipitated TRIM5 in both normoxic and hypoxic conditions and looked for DDX5 binding. DDX5 co-immunoprecipitated with TRIM5 in both normoxic and hypoxic conditions, although less DDX5 was observed in the hypoxic conditions presumably because the total levels of DDX5 were decreasing (**Figure 4I**). Finally, we used two siRNAs to deplete the levels of TRIM5 and asked if this would impact the repression of DDX5 in hypoxia. Loss of TRIM5 did not appear to impact DDX5 expression in normoxia but did lead to a partial restoration of DDX5 levels in hypoxia (**Figure 4J**). This data confirmed that TRIM5 is involved in DDX5 repression, but also suggested additional TRIM5-independent mechanisms. In support of this hypothesis, we observed a partial rescue of DDX5 repression in hypoxia in the presence of a

neddylation inhibitor, MLN4924, indicating the involvement of an alternative E3 ubiquitin ligase/s, from the Cullin-RING type family (**Supplementary Figure 5E**). Together, these data support the conclusion that TRIM5 is induced in response to hypoxia and can act as an E3 ligase for DDX5, but that additional mechanisms may contribute, including Cullin-RING type ligases, that ensure efficient repression of DDX5 in hypoxia.

We hypothesized that the repression of R-loop related genes in hypoxia and the loss of these factors could in part explain the increase in R-loops in hypoxic conditions [7]. Although it was possible that rescuing the expression of a single component of the R-loop interactome in hypoxia would have little impact, we investigated whether rescuing DDX5 in hypoxia could reduce the accumulation of R-loops in hypoxia. However, as R-loops are transcription dependent and DDX5 is a transcription co-factor, we first determined if increasing DDX5 in hypoxia increased this activity. We focused on the expression of E2F targets as DDX5 is a known co-factor of E2F1 and we have previously shown that some E2F target genes are repressed in hypoxia [35]. We overexpressed DDX5 in HCT116 cells and tested expression of known E2F target genes in hypoxia. As expected, we observed a clear decrease of MCM2, MCM4, MCM5, MCM6, MCM7 and CDC6 proteins in hypoxia, however we did not see any rescue when DDX5 was restored (**Supplementary Figure 6)**. This suggested that rescuing DDX5 in hypoxia is not likely to increase overall transcription levels, at least through E2F-dependent transcription. We then investigated the effect of restoring DDX5 expression in hypoxia on the levels of R-loops. DDX5 was expressed in HCT116 cells and exposed to hypoxia (<0.1% O_2), and the catalytic-dead mutant RNase $H1^{D210N}$ assay was used to visualize R-loops (**Figure 5A**) [36,37]. Surprisingly, we found that rescuing DDX5 in hypoxia led to a significant accumulation of R-loops. In contrast when we restored the expression of DHX9, R-loop levels were significantly reduced both in normoxia and in hypoxia (**Figure 5B-C**). To confirm this surprising finding, we verified the role of DDX5 in R-loops in hypoxia in a second

cell line, A549, and also made use of the DDX5 helicase mutant (DDX5^{NEAD}). Again, we found that when DDX5 expression was restored in cells exposed to hypoxia, the levels of R-loops increased further and importantly that this was dependent on DDX5 helicase activity (**Figure 5D**). These data demonstrate that in hypoxic conditions, the restoration of DDX5-mediated helicase activity increases R-loop levels and that this is specific to the DDX5 helicase, as over-expression of DHX9 abrogated R-loops.

DISCUSSION

We demonstrate that many genes involved in R-loop formation and resolution (the R-loop interactome) are repressed in hypoxic conditions, with the notable exception of SETX. Our ATACseq analysis suggests that in the majority of cases the repression of the R-loop interactome correlates with decreased chromatin accessibility, likely leading to reduced transcription. Changes in chromatin accessibility in hypoxia have been previously characterized in hypoxia-induced cardiac damage, adaptation to high-altitude, or cancer cell lines, and both chromatin condensation and increased open chromatin at various loci, including hypoxia-responsive genes, were reported [38–41]. Recently, ATACseq was also used to demonstrate that the type I interferon pathway is downregulated in hypoxia, and that this is dependent on decreased chromatin accessibility at genes with motifs for STAT1 and IRF3 [42]. Here, we found further pathways downregulated through this mechanism in hypoxia, including DNA repair, splicing and the R-loop interactome. It is plausible that the reduced expression of genes in all of these pathways contributes to R-loop levels in hypoxia.

Evidence to support the hypothesis that the repression of these genes is part of the biological response to hypoxia as opposed to an energy saving measure comes from our finding that in the case of DDX5, multiple mechanisms exist in hypoxia to reduce expression. While DDX5

mRNA was reduced in TCGA samples with significant levels of hypoxia, we found that DDX5 protein levels could decrease in response to hypoxia in the absence of decreased mRNA. This led to the identification of TRIM5 as an E3 ligase for DDX5 and the first demonstration of TRIM5 hypoxia-inducibility. Interestingly, a recent report showed that the lncRNA SLC2A4-AS1 can facilitate the interaction between DDX5 and TRIM25 leading to the degradation of DDX5 [43]. This finding supports our conclusion that DDX5 is likely targeted by multiple E3 ligases, including TRIM5 and 25, although the role of TRIM25 in hypoxia has not been tested. In addition, the induction of miR-462 and 731 in hypoxia in a HIF-dependent manner has been shown to repress DDX5 in zebrafish, further supporting our finding that multiple mechanisms exist to reduce DDX5 in hypoxia [44]. Surprisingly, whilst we predicted that loss of the R-loop interactome contributed to R-loop levels in hypoxia, we found that this was not a general response as rescuing DDX5 increased R-loops whilst the opposite effect was seen when DHX9 was restored. Notably our studies have focused on the global levels of R-loops and do not address changes at specific genomic locations.

Why restoring DDX5 expression in hypoxia leads to further R-loop accumulation above the level observed in hypoxia is unclear. Previous reports have all shown that expression of DDX5 leads to R-loop resolution i.e., a decrease in R-loop levels [15–19]. To our knowledge, expression of DDX5 in hypoxia is the first example of a context where DDX5 has been linked to R-loop accumulation. One hypothesis is that this is related to the changes in splicing also observed in these conditions as recruitment of spliceosome onto nascent mRNA attenuates R-loop formation [45]. In support of this, in a background of loss of key splicing factors over-expression of DHX9 has been shown to increase R-loop accumulation [46]. However, when we restored DHX9 in hypoxia, we found an almost complete abrogation of R-loops, although notably this also occurred in the normoxic samples, making the impact of DHX9 in hypoxia difficult to interpret.

A caveat to having chosen DDX5 as an exemplar from the R-loop interactome is that DDX5 has numerous functions which are independent of R-loops [12–14,47–49]. For example, it is plausible that repression of DDX5 could be a part of the biological adaption to reduced oxygen levels as shRNA-mediated depletion of DDX5 in lung cancer cells has been shown to lead to reduced oxygen consumption through changes in mitochondrial respiration, oxidative phosphorylation and reduced intracellular succinate [50].

One of the aspects of DDX5 which intrigued us was the finding that is overexpressed or amplified in a wide range of cancers [51]. Initially our finding that hypoxia leads to loss of DDX5 seemed contradictory to the finding that it is over-expressed in cancers. However, when considered together, this demonstrates that whilst hypoxic tumors express less DDX5, the levels are increased compared to normal tissues. This in turn suggests that the *DDX5* gene amplification in cancers could occur to compensate for the repressive effect of hypoxia on DDX5. Together our data highlight the significant energy-consuming processes a hypoxic cell employs to turn off the expression of specific genes such as DDX5 and, not surprisingly, that cancers circumvent this biological response.

METHODS

Cell lines and reagents

HCT116, RKO, U87, A549, MCF-7, MDA-231, DLD1, H1299, WI-38 and MRC5 cells (from ATCC) were cultured in DMEM with 10% FBS. OE21 and FLO1 were obtained from PHE culture collections and cultured in RPMI and DMEM, respectively, all supplemented with 10% FBS. GL261 mouse glioma cells stably expressing either pEGFP-N1 or tdTomato (luc+tdT+) were cultured in DMEM with 10% FBS with antibiotics (50 U/ml penicillin, 50 mg/ml

streptomycin) [52,53]. NBE1 were cultured in DMEM F12 advanced, glutamax and 1% FBS while ARPE-19 cells were cultured in DMEM F12 medium supplemented with 10% FBS (cells from Prof Geoff Higgins, University of Oxford). ReNCell CX, ReNCell VM (from Prof Eric O'Neill, University of Oxford). HCT116 p53+/+ and p53-/- cell lines were a gift from Prof Vogelstein (Johns Hopkins University, Baltimore, USA). DharmaFECT 1 transfection reagent (Dharmacon) was used for siRNA transfections according to the manufacturer's instructions; sequences are available in the SI. pSG5-myc, pSG5-mycDDX5 and pSG5-mycDDX5-NEAD plasmids were a kind gift from Prof. Frances Fuller-Pace (University of Dundee) and DHX9 plasmid from Dr Natalia Gromak (University of Oxford). ppyCAG_RNaseH1_D210N_V5 plasmid was obtained from Addgene (#111904). Plasmid transfection was carried out using jetPRIME® (Polyplus) transfection reagents according to the manufacturer's protocol.

Hypoxia and drug treatment

Cells were incubated at <0.1% O_2 in a Bactron chamber (Shel Lab) or at <0.1%-2% O_2 in a M35 Hypoxystation (Don Whitley) hypoxic chambers in the presence of 5% CO_2. The following drugs were used: 25 µg/ml Cycloheximide, 20 µM Emetine, 5 µM MG-132, 2 µM MLN-4924, 1 µM Ruxolitinib, 100 µg/ml RNAseA, $1x10^3$ U/ml IFNα, 100 µg/ml INFγ, 100 µM 5,6-dichloro-1-β-d-ribofuranosylbenzimidazole (DRB), 10 µM Camptothecin (CPT)

Western blotting

Cells were washed in PBS and lysed in SDS lysis buffer (10 mM Tris-Cl, pH 7.5, 0.1 mM EDTA, 0.1 mM EGTA, 0.5% SDS, 0.1 mM β-mercaptoethanol, protease/phosphatase inhibitors). After blocking in LiCOR blocking buffer the following primary antibodies were used: DDX5 (Pab204, kind gift from Prof. Frances Fuller-Pace; clone204, Sigma-Aldrich), DHX9 (ab26271, Abcam) TRIM5 (D-6, Santa Cruz), DDX17 (SQQ-K14, kind gift from Prof. Frances Fuller-Pace, Dundee, UK), p53 (DO-I, Santa Cruz), H3K4me3 (07-473, Millipore),

H3K9me3 (ab8898, Abcam), H3K27me3 (07-449, Millipore), H3 total (ab1791, Abcam) β-actin (AC-15, Santa Cruz), HIF-1α (610958, BD Biosciences), and GAPDH (6C5, Novus Biologicals). IRDye® 680 or IRDye® 800 secondary antibodies were used and the Odyssey infrared system (LI-COR) to visualize western blots.

Immunoprecipitation

Cells were washed in PBS and lysed with IP lysis buffer (1% NP-40, 150 mM NaCl, 20 mM HEPES, 0.5 mM EDTA, protease and phosphatase inhibitors cocktail (Roche)). Cellular extracts were incubated with TRIM5 antibody (AF3684, R&D systems) or IgG control (Millipore) with end-to-end rotation overnight at 4°C. Subsequently, 20 µl of pre-washed Protein G agarose beads (Millipore) were added for additional 2 h incubation. Beads were washed 3x in IP lysis buffer and immunoprecipitated complexes were eluted by boiling in 2xSDS sample buffer. Western blotting was carried on IP and input samples.

R-loop quantification

Cells transfected with RNase $H1^{D21ON}$ V5 were pre-extracted in ice-cold PBS/0.2% Triton-X 100 for 2 min, fixed in 4% paraformaldehyde for 10 min, permeabilized in 0.1% Triton-X 100 for 10 min and blocked with 1% BSA /FBS in PBS for 1 hour. Cells were then incubated with V5 antibody (R96025, ThermoFisher Scientific) followed by Alexa fluor mouse 488 secondary antibody (A11029, Invitrogen) for 1 hour at room temperature. Coverslips were mounted using mounting medium Prolong® Gold with DAPI (P36962, Invitrogen). Images were captured using a LSM710 confocal microscope (Carl Zeiss, Germany). Images processing and analysis was performed using Image J software. The V5 mean nuclear intensity signal was determined using the Image J plugin/algorithm, measured as previously [7]. A minimum of 100 cells were included per condition.

Immunohistochemistry and immunofluorescence on xenograft sections

Animal procedures involving HCT116 and OE21 xenografts were performed in accordance with current UK legislation and were approved by the University of Oxford Biomedical Services Ethical Review Committee, Oxford, UK. HCT116 and OE21 cells were grown as xenograft tumors as previously described [34]. Briefly, 6–8-week-old female athymic nude mice (BALB/c nude) (Charles River, UK) were injected subcutaneously into the flank with 5 × 10^6 HCT116 cells in serum-free DMEM. Or, 6–8-week-old female CD-1 nude mice (Charles River, UK) were injected subcutaneously into the flank with 5 × 10^6 OE21 cells in 50% (v/v) matrigel and serum-free RPMI. 2 h before the tumor was harvested, mice were injected intraperitoneally with 60 mg/kg of pimonidazole. Tumors were harvested before reaching 500 mm^3 (according to the formula V=WxDxLxπ/6). Hypoxic regions were visualized by pimonidazole staining with hypoxyprobe 1 antibody (clone 4.3.11.3, Hypoxyprobe) after dewaxing and antigen retrieval with 10 mM sodium citrate buffer (pH 6.0). In addition, serial sections were stained for DDX5 (pAb204, Millipore), or no primary antibody (negative control), followed by HRP-conjugated secondary antibody incubation. Staining was developed with 3,3′-Diaminobenzidine (DAB, Vector Labs), and nuclei were counterstained with hematoxylin. Images were obtained using an Aperio Scanner (Leica Biosystems).

Orthotopic mouse GL261 glioma growth was conducted under the protocol 1019/2020 approved by the Local Ethics Committee for Animal Experimentation at the Nencki Institute of Experimental Biology in Warsaw. Male C57BL/6 mice (12 weeks) were anesthetized with 4% isofluorane and maintained at 1.5% isofluorane in oxygen during the tumor implantation procedure. 8x10^4 luc+tdT+ GL261 glioma cells in 1 µl of DMEM were inoculated into a right striatum at the rate of 0.25 µL per minute using a stereotactic apparatus. The coordinates for injection were +1 mm anterior-posterior, -2 mm lateral and -3 mm dorsal-ventral in relation to bregma. 25 days post implantation animals were intraperitoneally injected with 60 mg/kg of

pimonidazole and 2 h later were anesthetized, sacrificed and perfused with PBS and subsequently with 4% paraformaldehyde (PFA) in PBS. Brains with tumors were then removed and fixed additionally with 4% PFA in PBS for 24 h, followed by immersion in 30% sucrose for 48 h and mounting in OCT freezing medium on dry ice. 10 µm coronal sections were collected using a cryostat. Sections were subjected to an antigen retrieval with 10 mM sodium citrate buffer (pH 6.0) and co-staining with hypoxyprobe 1 antibody and DDX5 (ab126730, Abcam) antibody was carried out. Nuclei were counterstained with DAPI. Images were acquired using a Zeiss LSM800 confocal microscope.

qPCR

RNA samples were prepared using TRIzol (Invitrogen/Life Technologies). cDNA was synthesized from total RNA using the Verso Kit (Thermo Scientific). qPCR was performed with the SYBR Green PCR Master Mix Kit (Applied Biosystems) in a 7500 FAST Real-Time PCR thermocycler with v2.0.5 software (Applied Biosystems). Primer sequences are included in the supplementary information. 18S was used as housekeeping gene. mRNA fold change was calculated using a $2^{-\Delta\Delta Ct}$ method. The qPCR graphs show the mean ± SEM of 3 biological replicates and statistical significance analysed with two-tailed student t-tests for each gene.

Gene expression correlations in TCGA datasets

RNA-sequencing data (RNA Seq V2 RSEM) for 382 colorectal adenocarcinoma, 166 glioblastoma, 408 bladder urothelial carcinoma, 1100 breast invasive carcinoma, 501 lung squamous cell carcinomas and 517 lung adenocarcinomas patient sample datasets from the TCGA project were accessed through cBioportal (http://www.cbioportal.org/). To examine the correlation of DDX5 against hypoxia signature, raw data for each sequenced gene were rescaled to set the median equal to 1, and hypoxia signature was determined by quantifying the

median expression of genes from the hypoxic signature [54]. Log10 conversion of the hypoxia signature was plotted against Log10 conversion of raw data for DDX5 (also rescaled to set the median equal to 1). Similarly, to test the correlation of TRIM5 with tumour-associated hypoxia-induced p53-activity (referred to as hypoxic p53 target genes in Figure S8D), raw data for each sequenced gene were rescaled to set the median equal to 1, and hypoxic p53 targets were determined by quantifying the median expression of 6 p53 target genes associated with hypoxia-induced p53 activity (encoding BTG2, CYFIP2, INPP5D, KANK3, PHLDA3 and SULF2) [34]. Correlations and statistical significance were determined by calculating Spearman's rho rank correlation coefficients and two-tailed P values using Hmisc package in R studio.

ATACseq sequencing and data processing

ATACseq was performed as previously described with some modifications [22]. While still in hypoxic conditions, GL261 cells were fixed with 1% formaldehyde (Thermo Scientific) for 10 min and then quenched with 0.125 M glycine for 5 min at room temperature. After return to normal conditions (21% O_2), cells were counted and 25,000 cells were washed and subsequently lysed in cold lysis buffer (10 mM Tris-HCl, pH 7.4, 10 mM NaCl, 3 mM MgCl2 and 0.1% IGEPAL CA-630) for 5 min on ice. Cells were then centrifuged at 500xg for 8 min and cell pellets resuspended in transposition reaction according to the standard ATACseq protocol using 2.5 ul of Tn5 enzyme per 25 000 of cells [55]. After transposition cells were centrifuged and reverse crosslinked (50 mM Tris-Cl, 1 mM EDTA, 1% SDS, 0.2 M NaCl, 200 µg/ml proteinase K) at 65°C with an overnight shaking at 1000 rpm. Zymo DNA Clean & Concentrator-5 columns (ZymoResearch) were used to purify DNA and the sequencing libraries were prepared according to the original ATACseq protocol [55]. The ATACseq libraries were assessed for appropriate quality using Bioanalyzer 2100 and subjected to paired-end sequencing (2x76 bp) using NovaSeq 6000 (Illumina) at the Laboratory of Sequencing (Nencki

Institute). The quality of raw fastq data was assessed using FASTQC software (https://www.bioinformatics.babraham.ac.uk/projects/fastqc/). Reads were trimmed using Trimmomatic to remove adapter and transposase sequence with option "sliding window 5:20" and with a cut off from 5' and 3' end set to 3 and 15, respectively [56]. Reads with a length of less than 50 bp were discarded. Then paired-end reads were aligned to mm10 using Bowtie2 aligner v2.2.5 with parameters set to –very sensitive and -X2000 [57]. Duplicate reads were subsequently removed with Picard (http://picard.sourceforge.net) and reads mapping to the mitochondrial genome were also removed. Only properly paired reads with mapping quality score (MAPQ) > 30 were kept for downstream analysis using Samtools view with option -q 30 [58]. Peaks were called using MACS2 v.2.1.1.2 with parameters set to -f BAPME -q 0.001 –nomodel –shift 0 [58]. The obtained peaks were then filtered for peaks overlapping mm10 ENCODE blacklisted genomic regions. To visualize the overlap of open genomic regions (peaks) from different conditions, the makeVennDiagram function from the ChIPpeakAnno package was used with minoverlap parameter set to 200 [59]. All sequencing track figures were generated by IGV using a normalized bigWig file created with deepTools (bamCoverage) and normalized to genome coverage - RPGC [60,61]. ATACseq data files are available at https://www.ncbi.nlm.nih.gov/geo under accession number GSE200757.

Differential analysis of ATACseq peaks

Changes in chromatin accessibility were assessed using DESeq2 [62] . To create a set of consensus ATAC peaks for the read count matrix, the following steps were performed. First, peaks for all replicates in a given condition were intersected and only peaks with overlap > 200 bp were included. Then obtained peaks from all conditions were merged with reduction of overlapping regions using the "reduce" function from GenomicRanges package to generate consensus peak lists [63]. Peaks with FDR < 0.05 and |log2 fold change| >= 0.6 were classified as significantly different.

Annotation for differential ATACseq peaks to genomic features

The peaks were annotated to genomic features using ChIPseeker with promoter region defined as +/- 2,000 bp around transcription start site (TSS) [64]. Each peak was annotated to only one genomic feature according to the default annotation priority in ChIPseeker. To obtain all the genes for which peaks were assigned around their promoter region, a custom-written script in R was used based on biomaRt and GenomicRanges packages [63,65]. Functional enrichment analysis of differentially accessible regions nearby genes was performed using Gene Ontology, (GO) KEGG and Reactome databases [25–27].

Statistical analysis and data processing

Statistical analyses for qPCRs, immunofluorescent analysis of DDX5 expression and R-loop quantification were performed using GraphPad Prism software (GraphPad Software Inc.). A scheme in Figure 3E was drawn with BioRender.com under the license agreement number AG23UKM2W6. As indicated in figure legends, statistical tests included two-tailed student t-tests ns = non-significant, *p ≤0.05, **p ≤ 0.01, ***p ≤ 0.001, ****p ≤ 0.0001.

AUTHORS CONTRIBUTIONS

KBL co-conceived the project; conceived, designed, performed or supervised, interpreted the majority of the experiments; and wrote the manuscript. MD performed ATACseq experiments, analyses and validation; and contributed to the writing of the manuscript. HE performed R-loop assays. J(utta)M performed qPCR analyses. EB contributed to the writing of the manuscript. AJG provided feedback and supervision. J(akub)M assisted with the ATACseq analyses and advised on the manuscript. BK advised on the manuscript and facilitated ATACseq experiments. EMH co-conceived the project; conceived, designed, and interpreted

the majority of the experiments; and wrote the manuscript. All authors commented on the manuscript.

ACKNOWLEDGEMENTS

Thank you to Monica Olcina and Tiffany Ma (University of Oxford) for their insightful feedback on our manuscript. KBL and EB were supported by a CRUK grant C5255/A23755 (awarded to EMH). KBL was also supported by CRUKDF 0715-KL grant (awarded to KBL and EMH). MD and KBL were supported by National Science Centre (Poland) grant 2019/33/B/NZ1/01556 (awarded to KBL). HE was supported by Medical Research Council - UKRI grant MC _UU_00001/8 (awarded to AJG). We acknowledge Ms Beata Kaza for preparing GL261 cryo-sections. We acknowledge Mr Paweł Segit, Mr Karol Jacek and Dr Adria-Jaume Roura Canalda for guidance on ATACseq data analysis. We acknowledge Ms Paulina Szadkowska, Dr Bartlomiej Gielniewski and Dr Bartosz Wojtas for sequencing the ATACseq samples.

The authors disclose no potential conflicts of interest.

FIGURE LEGENDS

Figure 1. Oxygen-dependent chromatin alterations lead to a loss of promoter accessibility of numerous pathways, including RNA processing factors.

A. GL261 cells was exposed to 16 h of 21, 1 or <0.1% O_2 and subjected to western blotting for the histone modifications indicated and HIF-1α hypoxia control.

B. GL261 cells were exposed to 16 h of normoxia (21% O_2) or two conditions of hypoxia (1 and <0.1% O_2). Samples were fixed and ATACseq carried out. Principal component analysis of ATACseq peaks for the three oxygen tensions is shown.

C. Venn diagram showing hypoxia-specific or common ATACseq peaks detected in all oxygen conditions from **B**. The percentage of peaks in the total amount of peaks is shown for each condition (in brackets).

D. A volcano plot showing differentially altered ATACseq peaks in 1% O_2 versus 21% O_2. Statistically significant peaks with FDR < 0.05 and |log2 fold change| ≥ 0.6 are marked in blue.

E. A volcano plot showing differentially altered ATACseq peaks in <0.1% O_2 versus 21% O_2. Statistically significant peaks with FDR < 0.05 and |log2 fold change| ≥ 0.6 are marked in yellow.

F. A bar chart showing differentially regulated ATACseq peaks from parts **D** and **E** annotated to distinct genomic regions at 1% or <0.1% O_2 in relation to normoxic control. "Up" or "Down" marks significantly increased or decreased peaks, respectively, for each hypoxic condition in relation to normoxia.

G. Top 10 Gene Ontology (GO) pathways (based on the highest gene count) associated with genes that had decreased ATACseq peaks at their promoters. Adjusted *P* value indicates statistical significance for each pathway shown.

H. A volcano plot showing differentially regulated ATACseq peaks at the gene promoters in cells treated with <0.1% O_2, with significantly up-regulated 251 peaks and 3030 downregulated peaks. Statistically significant peak changes were annotated with green dots (FDR < 0.05 and |log2 fold change| ≥ 0.6). Black dots mark all significantly downregulated peaks for promoters

of genes from the GO pathway "RNA splicing" (GO:0008380) and some names of these genes were indicated (full list in **Supplementary Table 4**).

I. A qPCR validation of hypoxia-dependent repression of splicing factors indicated in **H**. *Vegfa* and *Slc2a1* were used as positive hypoxia-inducible controls.

Figure 2. DDX5 is repressed in hypoxic conditions *in vitro* and *in vivo*.

A. A volcano plot from **1H** highlighting repressed promoters in R-loop-interacting helicases at severe hypoxia. The graph showing genes with significantly increased and decreased ATACseq signals within their promoter regions at <0.1% O_2 in relation to 21% O_2 with green dots representing all significantly regulated peaks (FDR < 0.05 and |log2 fold change| ≥ 0.6). The dots marked in black highlight the top R-loop-interacting factors shortlisted from [29].

B. ATACseq peak profiles (from Integrative Genomics Viewer, IGV) showing repressed chromatin at the promoters of Ddx5 and Dhx9 genes in GL261 cells.

C-G. GL261, A549, RKO, OE21, MRC5 and HCT116 cell lines were exposed to hypoxia (Hyp, 0.1% O_2) for the times indicated followed by western blotting for DDX5 as well as HIF-1α (hypoxic marker and β-actin (loading control). In addition, in part **C**, cells were exposed to reoxygenation (with 21% O_2) for the indicated times following hypoxia.

H. HCT116 cells were exposed to the hypoxic conditions indicated, or hypoxia mimetics $CoCl_2$ (150 μM) or DFO (100 μM) for the times indicated. Western blotting was then carried out using the antibodies shown.

I. Sequential sections from HCT116 and OE21 tumour xenografts using the cell lines indicated (HCT116 or OE21) were stained for hypoxia with anti-pimonidazole hyoxyprobe-1 (PIMO)

and DDX5 antibodies. Nuclei were counterstained with hematoxylin Scale bar = 50 μm. The outline of PIMO-positive (brown) staining is shown by the dashed white line.

J. PFA-fixed GL261 tumor xenografts were sectioned and subjected to immunofluorescent staining for hypoxia (PIMO) and DDX5. Nuclei were counterstained with DAPI. Scale bar = 100 μm. The outline of PIMO-positive (FITC) staining is shown by the dashed white line.

K. Mean fluorescence intensity ± standard deviation of DDX5 signal (labeled with Alexa Fluor-647) in GL261 tumors from **J** was measured in hypoxic (PIMO+ve) and normoxic (PIMO-ve) image areas using ZEN2 software (Zeiss). 22 hypoxic areas and 31 normoxic areas were analyzed and two-tailed non-parametric Mann-Whitney test shows statistical significance (*P* value 0.007, **)

Figure 3. DDX5 expression in hypoxia is controlled transcriptionally and post-translationally.

A. Expression of *DDX5* (mRNA) was correlated with hypoxia metagene signature in the indicated TCGA cancer patient cohorts: Breast invasive carcinoma (Breast), Colorectal adenocarcinoma (Colorectal), Glioblastoma, Bladder urothelial carcinoma (Bladder), Lung adenocarcinoma and Lung squamous cell carcinoma. The numbers of patient samples are shown in brackets. Spearman's rank correlation coefficient and *P* values are shown for the Log10 median expression of *DDX5* and hypoxic signature.

B. The indicated cell lines were exposed to hypoxia (<0.1% O_2) for 18 h. Expression of *DDX5* and *VEGF* mRNA was then determined by qPCR and normalized to *18S*. Statistical significance was calculated with two-tailed student t-test for each cell line (* P<0.05, ** P<0.01, *** P<0.001, ns non-significant).

C. HCT116 cells were exposed to hypoxia (Hyp, <0.1% O_2) and 5 μM MG-132 as indicated and western blotting was carried out with the antibodies shown.

D. HCT116 cells were treated with 25 μg/ml cycloheximide (CHX) in hypoxic (Hyp, <0.1% O_2) or normoxic (Norm, 21% O_2) conditions for the times indicated and analysed with western blotting.

E. A scheme proposing a hypoxia-inducible E3 ubiquitin ligase involved in the degradation of DDX5. Created with BioRender.com

Figure 4. The TRIM5 E3-ligase is hypoxia-inducible and contributes to DDX5 degradation.

A. RKO cells were exposed to hypoxia (Hyp, <0.1% O_2) for the times shown and mRNA expression of *TRIM5*, *TRIM21* and *VEGFA* was analyzed by qPCR and normalized to 18S housekeeping gene. Statistical significance was determined with two-tailed student t-test for each gene by comparing control and specific time in hypoxia (* P<0.05, *** P<0.001, *** P<0.0001, ns non-significant).

B-C. RKO and HCT116 cells were exposed to hypoxia for the times indicated and subjected to western blotting with TRIM5 and DDX5 antibodies.

D. Expression of DDX5 and TRIM5 proteins was analyzed in non-malignant (labeled in green) and cancer cell lines (labeled in red) as indicated, by western blotting. Histone H3 and β-actin were used as loading controls.

E. HCT116 cells were exposed to <0.1 or 2% O_2 for the times indicated and were subjected to western blotting with the antibodies indicated.

F-G. OE21 cells were exposed to hypoxia for the times indicated and subjected to a qPCR (G) and western blotting (H) analysis. *18S* served as a housekeeping gene in the qPCR analysis.

H. HCT116$^{p53+/+}$ and $^{p53-/-}$ cells were exposed to 18 h of hypoxia (Hyp, <0.1% O_2) and *TRIM5* expression was analysed relative to 18S. *INPP5D* expression is shown as a positive control for p53-dependent hypoxia-inducible target gene. Bar graphs show mean expression and SEM of 3 biological replicates. Statistical significance was determined with two-tailed student t-test for each gene and conditions indicated (* P<0.05, ** P<0.01).

I. HCT116 cells were exposed to 6 h of hypoxia (<0.1% O_2) or non-treated (Norm) and lysates were subjected to immunoprecipitation (IP) with polyclonal goat anti-TRIM5 antibody or goat IgG control. TRIM5 and DDX5 interaction was determined in IP samples by western blotting and compared to the input, as shown.

J. HCT116 cells were transfected with non-targeting siRNA control (Scr), two different siRNA duplexes against TRIM5 (siTRIM5#1 and siTRIM5#2) or were Mock transfected (no siRNA) and the next day cells were exposed to 16 h of hypoxia (<0.1% O_2). Protein expression was analyzed by western blotting.

Figure 5. Rescuing DDX5 expression in hypoxia leads to accumulation of R-loops.

A. HCT116 were co-transfected with myc-tagged DDX5 together with RNase H1^{D210N} and exposed to hypoxia (18 h) followed by western blotting.

B. HCT116 cells were transfected as in part A, staining for V5 was then carried out. Representative images are shown (scale bar: 10 μm). V5 staining in green, DAPI (blue) shows the nucleus.

C. Nuclear intensity of V5 staining (R-loops) was determined. Data represent mean expression and SEM from three independent experiments. Statistical significance was calculated with unpaired student t-test for each indicated condition (* $P<0.05$).

D. A549 cells were co-transfected with RNase $H1^{D210N}$ together with myc-tagged DDX5 or myc-tagged $DDX5^{NEAD}$ or with DHX9 and exposed to hypoxia for 18 hours. CPT or DRB were used as a positive and negative controls for R-loops, respectively. Analysis of R-loop fluorescent intensity was analyzed as in C. Data represent mean expression and SEM from four independent experiments. Statistical significance was determined with unpaired student t-test for each indicated condition (*$P<0.05$).

REFERENCES

1. Raymond, J. & Segrè, D. The effect of oxygen on biochemical networks and the evolution of complex life. *Science (80-.).* **311**, (2006).

2. Liao, C. & Zhang, Q. Understanding the Oxygen-Sensing Pathway and Its Therapeutic Implications in Diseases. *American Journal of Pathology* vol. 190 (2020).

3. Hammond, E. M. *et al.* The Meaning, Measurement and Modification of Hypoxia in the Laboratory and the Clinic. *Clin. Oncol.* **26**, (2014).

4. Chan, N. *et al.* Contextual synthetic lethality of cancer cell kill based on the tumor microenvironment. *Cancer Res.* **70**, (2010).

5. Santos-Pereira, J. M. & Aguilera, A. R loops: New modulators of genome dynamics and function. *Nature Reviews Genetics* vol. 16 (2015).

6. Crossley, M. P., Bocek, M. & Cimprich, K. A. R-Loops as Cellular Regulators and

Genomic Threats. *Molecular Cell* vol. 73 (2019).

7. Ramachandran, S. *et al.* Hypoxia-induced SETX links replication stress with the unfolded protein response. *Nat. Commun.* **12**, (2021).

8. Olcina, M. M. *et al.* Replication stress and chromatin context link ATM activation to a role in DNA replication. *Mol. Cell* **52**, (2013).

9. Batie, M. *et al.* Hypoxia induces rapid changes to histone methylation and reprograms chromatin. *Science (80-.).* **363**, (2019).

10. Olcina, M. M. *et al.* H3K9me3 facilitates hypoxia-induced p53-dependent apoptosis through repression of APAK. *Oncogene* **35**, (2016).

11. Brady, L. K. *et al.* Transcriptome analysis of hypoxic cancer cells uncovers intron retention in EIF2B5 as a mechanism to inhibit translation. *PLoS Biol.* **15**, (2017).

12. Giraud, G., Terrone, S. & Bourgeois, C. F. Functions of DEAD box RNA helicases DDX5 and DDX17 in chromatin organization and transcriptional regulation. *BMB Reports* vol. 51 (2018).

13. Dardenne, E. *et al.* RNA Helicases DDX5 and DDX17 Dynamically Orchestrate Transcription, miRNA, and Splicing Programs in Cell Differentiation. *Cell Rep.* **7**, (2014).

14. Geißler, V., Altmeyer, S., Stein, B., Uhlmann-Schiffler, H. & Stahl, H. The RNA helicase Ddx5/p68 binds to hUpf3 and enhances NMD of Ddx17/p72 and Smg5 mRNA. *Nucleic Acids Res.* **41**, (2013).

15. Villarreal, O. D., Mersaoui, S. Y., Yu, Z., Masson, J. Y. & Richard, S. Genome-wide R-loop analysis defines unique roles for DDX5, XRN2, and PRMT5 in DNA/RNA

hybrid resolution. *Life Sci. Alliance* **3**, (2020).

16. Kang, H. J. *et al.* Thrap3 promotes R-loop resolution via interaction with methylated DDX5. *Exp. Mol. Med.* **53**, (2021).

17. Yu, Z. *et al.* DDX5 resolves R-loops at DNA double-strand breaks to promote DNA repair and avoid chromosomal deletions. *NAR Cancer* **2**, (2020).

18. Mersaoui, S. Y. *et al.* Arginine methylation of the DDX 5 helicase RGG / RG motif by PRMT 5 regulates resolution of RNA:DNA hybrids . *EMBO J.* **38**, (2019).

19. Sessa, G. *et al.* BRCA2 promotes DNA-RNA hybrid resolution by DDX5 helicase at DNA breaks to facilitate their repair‡. *EMBO J.* **40**, (2021).

20. Pombo Antunes, A. R. *et al.* Single-cell profiling of myeloid cells in glioblastoma across species and disease stage reveals macrophage competition and specialization. *Nat. Neurosci.* **24**, (2021).

21. Dobrynin, G. *et al.* KDM4A regulates HIF-1 levels through H3K9me3. *Sci. Rep.* **7**, (2017).

22. Chen, X. *et al.* ATAC-see reveals the accessible genome by transposase-mediated imaging and sequencing. *Nat. Methods* **13**, (2016).

23. Klemm, S. L., Shipony, Z. & Greenleaf, W. J. Chromatin accessibility and the regulatory epigenome. *Nature Reviews Genetics* vol. 20 (2019).

24. Kouzarides, T. Chromatin Modifications and Their Function. *Cell* vol. 128 (2007).

25. Carbon, S. *et al.* Expansion of the gene ontology knowledgebase and resources: The gene ontology consortium. *Nucleic Acids Res.* **45**, (2017).

26. Kanehisa, M., Goto, S., Kawashima, S., Okuno, Y. & Hattori, M. The KEGG resource for deciphering the genome. *Nucleic Acids Res.* **32**, (2004).

27. Jassal, B. *et al.* The reactome pathway knowledgebase. *Nucleic Acids Res.* **48**, (2020).

28. Choudhry, H. & Harris, A. L. Advances in Hypoxia-Inducible Factor Biology. *Cell Metabolism* vol. 27 (2018).

29. Cristini, A., Groh, M., Kristiansen, M. S. & Gromak, N. RNA/DNA Hybrid Interactome Identifies DXH9 as a Molecular Player in Transcriptional Termination and R-Loop-Associated DNA Damage. *Cell Rep.* **23**, (2018).

30. Li, Y. *et al.* An integrated bioinformatics platform for investigating the human E3 ubiquitin ligase-substrate interaction network. *Nat. Commun.* **8**, (2017).

31. Asaoka, K. *et al.* A retrovirus restriction factor TRIM5α is transcriptionally regulated by interferons. *Biochem. Biophys. Res. Commun.* **338**, (2005).

32. Quintás-Cardama, A. *et al.* Preclinical characterization of the selective JAK1/2 inhibitor INCB018424: Therapeutic implications for the treatment of myeloproliferative neoplasms. *Blood* **115**, (2010).

33. Arnaiz, E. & Harris, A. L. Role of Hypoxia in the Interferon Response. *Front. Immunol.* **13**, 1–14 (2022).

34. Leszczynska, K. B. *et al.* Hypoxia-induced p53 modulates both apoptosis and radiosensitivity via AKT. *J. Clin. Invest.* **125**, (2015).

35. Pires, I. M. *et al.* Effects of acute versus chronic hypoxia on DNA damage responses and genomic instability. *Cancer Res.* **70**, (2010).

36. Chen, L. *et al.* R-ChIP Using Inactive RNase H Reveals Dynamic Coupling of R-loops

with Transcriptional Pausing at Gene Promoters. *Mol. Cell* **68**, (2017).

37. Teloni, F. *et al.* Efficient Pre-mRNA Cleavage Prevents Replication-Stress-Associated Genome Instability. *Mol. Cell* **73**, (2019).

38. Batie, M., Frost, J., Shakir, D. & Rocha, S. Regulation of chromatin accessibility by hypoxia and HIF. *Biochem. J.* **479**, 767–786 (2022).

39. Ward, M. C., Banovich, N. E., Sarkar, A., Stephens, M. & Gilad, Y. Dynamic effects of genetic variation on gene expression revealed following hypoxic stress in cardiomyocytes. *Elife* **10**, (2021).

40. Li, Y. *et al.* Acetate supplementation restores chromatin accessibility and promotes tumor cell differentiation under hypoxia. *Cell Death Dis.* **11**, (2020).

41. Xin, J. *et al.* Chromatin accessibility landscape and regulatory network of high-altitude hypoxia adaptation. *Nat. Commun.* **11**, (2020).

42. Miar, A. *et al.* Hypoxia induces transcriptional and translational downregulation of the type i IFN pathway in multiple cancer cell types. *Cancer Res.* **80**, (2020).

43. Yuan, J. *et al.* LncRNA SLC26A4-AS1 suppresses the MRN complex-mediated DNA repair signaling and thyroid cancer metastasis by destabilizing DDX5. *Oncogene* **39**, (2020).

44. Huang, C. X. *et al.* The zebrafish miR-462/miR-731 cluster is induced under hypoxic stress via hypoxia-inducible factor 1α and functions in cellular adaptations. *FASEB J.* **29**, (2015).

45. Bonnet, A. *et al.* Introns Protect Eukaryotic Genomes from Transcription-Associated Genetic Instability. *Mol. Cell* **67**, (2017).

46. Chakraborty, P., Huang, J. T. J. & Hiom, K. DHX9 helicase promotes R-loop formation in cells with impaired RNA splicing. *Nat. Commun.* **9**, (2018).

47. Mazurek, A. *et al.* DDX5 regulates DNA replication and is required for cell proliferation in a subset of breast cancer cells. *Cancer Discov.* **2**, (2012).

48. Nicol, S. M. *et al.* The RNA helicase p68 (DDX5) is selectively required for the induction of p53-dependent p21 expression and cell-cycle arrest after DNA damage. *Oncogene* **32**, (2013).

49. Nyamao, R. M., Wu, J., Yu, L., Xiao, X. & Zhang, F. M. Roles of DDX5 in the tumorigenesis, proliferation, differentiation, metastasis and pathway regulation of human malignancies. *Biochimica et Biophysica Acta - Reviews on Cancer* vol. 1871 (2019).

50. Xing, Z., Russon, M. P., Utturkar, S. M. & Tran, E. J. The RNA helicase DDX5 supports mitochondrial function in small cell lung cancer. *J. Biol. Chem.* **295**, (2020).

51. Dai, T. Y. *et al.* P68 RNA helicase as a molecular target for cancer therapy. *Journal of Experimental and Clinical Cancer Research* vol. 33 (2014).

52. Sliwa, M. *et al.* The invasion promoting effect of microglia on glioblastoma cells is inhibited by cyclosporin A. *Brain* **130**, (2007).

53. Ochocka, N. *et al.* Single-cell RNA sequencing reveals functional heterogeneity of glioma-associated brain macrophages. *Nat. Commun.* **12**, (2021).

54. Buffa, F. M., Harris, A. L., West, C. M. & Miller, C. J. Large meta-analysis of multiple cancers reveals a common, compact and highly prognostic hypoxia metagene. *Br. J. Cancer* **102**, (2010).

55. Buenrostro, J. D., Wu, B., Chang, H. Y. & Greenleaf, W. J. ATAC-seq: A method for assaying chromatin accessibility genome-wide. *Curr. Protoc. Mol. Biol.* **2015**, (2015).

56. Bolger, A. M., Lohse, M. & Usadel, B. Trimmomatic: A flexible trimmer for Illumina sequence data. *Bioinformatics* **30**, (2014).

57. Langmead, B. & Salzberg, S. L. Fast gapped-read alignment with Bowtie 2. *Nat. Methods* **9**, (2012).

58. Danecek, P. *et al.* Twelve years of SAMtools and BCFtools. *Gigascience* **10**, (2021).

59. Zhu, L. J. *et al.* ChIPpeakAnno: A Bioconductor package to annotate ChIP-seq and ChIP-chip data. *BMC Bioinformatics* **11**, (2010).

60. Ramírez, F. *et al.* deepTools2: a next generation web server for deep-sequencing data analysis. *Nucleic Acids Res.* **44**, (2016).

61. Robinson, J. T. *et al.* Integrative genomics viewer. *Nature Biotechnology* vol. 29 (2011).

62. Love, M. I., Huber, W. & Anders, S. Moderated estimation of fold change and dispersion for RNA-seq data with DESeq2. *Genome Biol.* **15**, (2014).

63. Lawrence, M. *et al.* Software for Computing and Annotating Genomic Ranges. *PLoS Comput. Biol.* **9**, (2013).

64. Yu, G., Wang, L. G. & He, Q. Y. ChIP seeker: An R/Bioconductor package for ChIP peak annotation, comparison and visualization. *Bioinformatics* **31**, (2015).

65. Durinck, S., Spellman, P. T., Birney, E. & Huber, W. Mapping identifiers for the integration of genomic datasets with the R/ Bioconductor package biomaRt. *Nat. Protoc.* **4**, (2009).

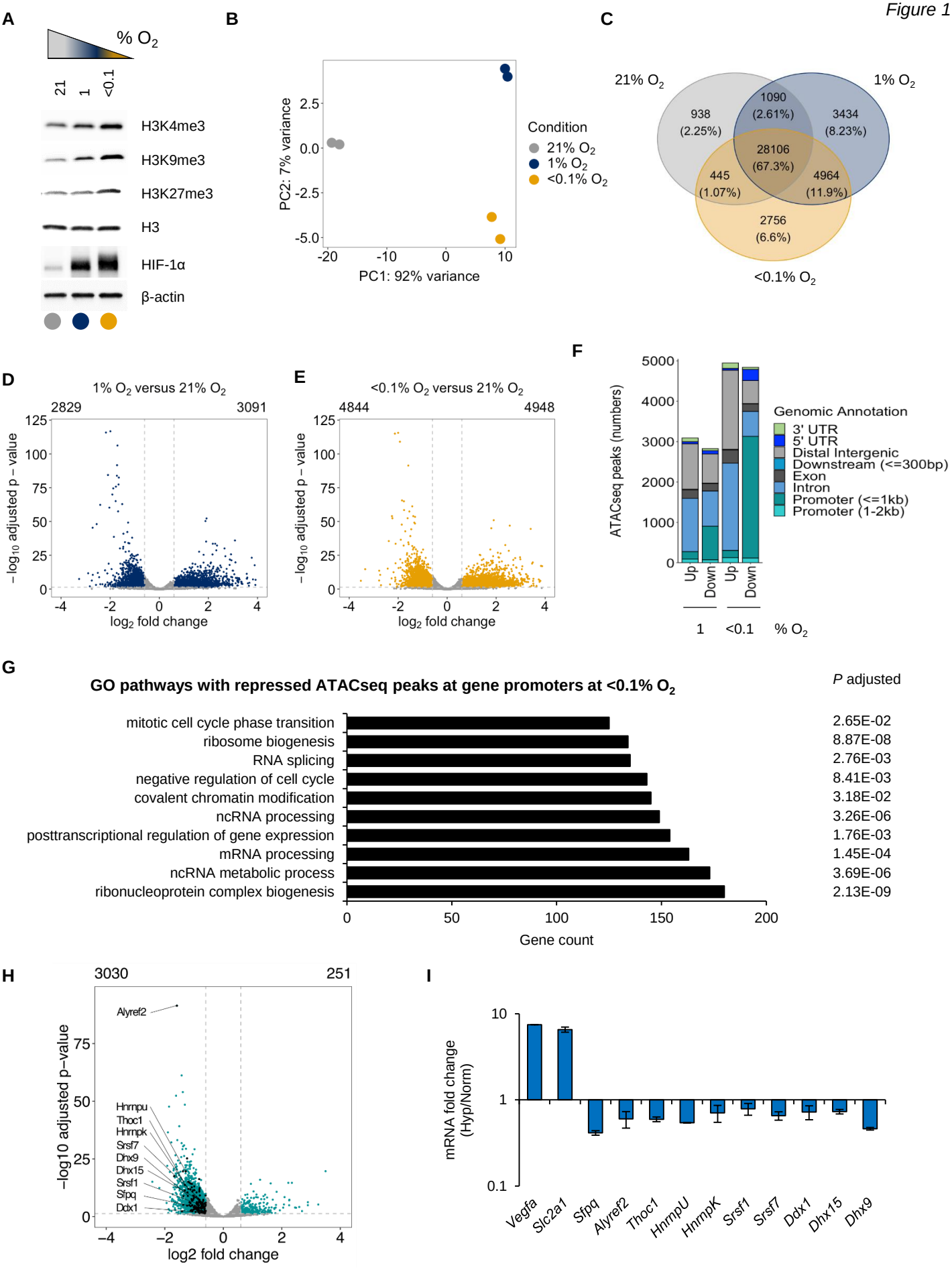
A
% O2
21
1
<0.1
H3K4me3
H3K9me3
H3K27me3
H3
HIF-1α
β-actin
B
PC2: 7% variance
PC1: 92% variance
Condition
21% O2
1% O2
<0.1% O2
C
21% O2
1% O2
<0.1% O2
938 (2.25%)
1090 (2.61%)
3434 (8.23%)
28106 (67.3%)
445 (1.07%)
4964 (11.9%)
2756 (6.6%)
D
1% O2 versus 21% O2
2829
3091
−log10 adjusted p − value
log2 fold change
E
<0.1% O2 versus 21% O2
4844
4948
−log10 adjusted p − value
log2 fold change
F
ATACseq peaks (numbers)
Genomic Annotation
3' UTR
5' UTR
Distal Intergenic
Downstream (<=300bp)
Exon
Intron
Promoter (<=1kb)
Promoter (1-2kb)
Up
Down
Up
Down
1
<0.1
% O2
G
GO pathways with repressed ATACseq peaks at gene promoters at <0.1% O2
P adjusted
mitotic cell cycle phase transition 2.65E-02
ribosome biogenesis 8.87E-08
RNA splicing 2.76E-03
negative regulation of cell cycle 8.41E-03
covalent chromatin modification 3.18E-02
ncRNA processing 3.26E-06
posttranscriptional regulation of gene expression 1.76E-03
mRNA processing 1.45E-04
ncRNA metabolic process 3.69E-06
ribonucleoprotein complex biogenesis 2.13E-09
Gene count
H
3030
251
Alyref2
Hnrnpu
Thoc1
Hnrnpk
Srsf7
Dhx9
Dhx15
Srsf1
Sfpq
Ddx1
−log10 adjusted p−value
log2 fold change
I
mRNA fold change (Hyp/Norm)
Vegfa
Slc2a1
Sfpq
Alyref2
Thoc1
HnrnpU
HnrnpK
Srsf1
Srsf7
Ddx1
Dhx15
Dhx9

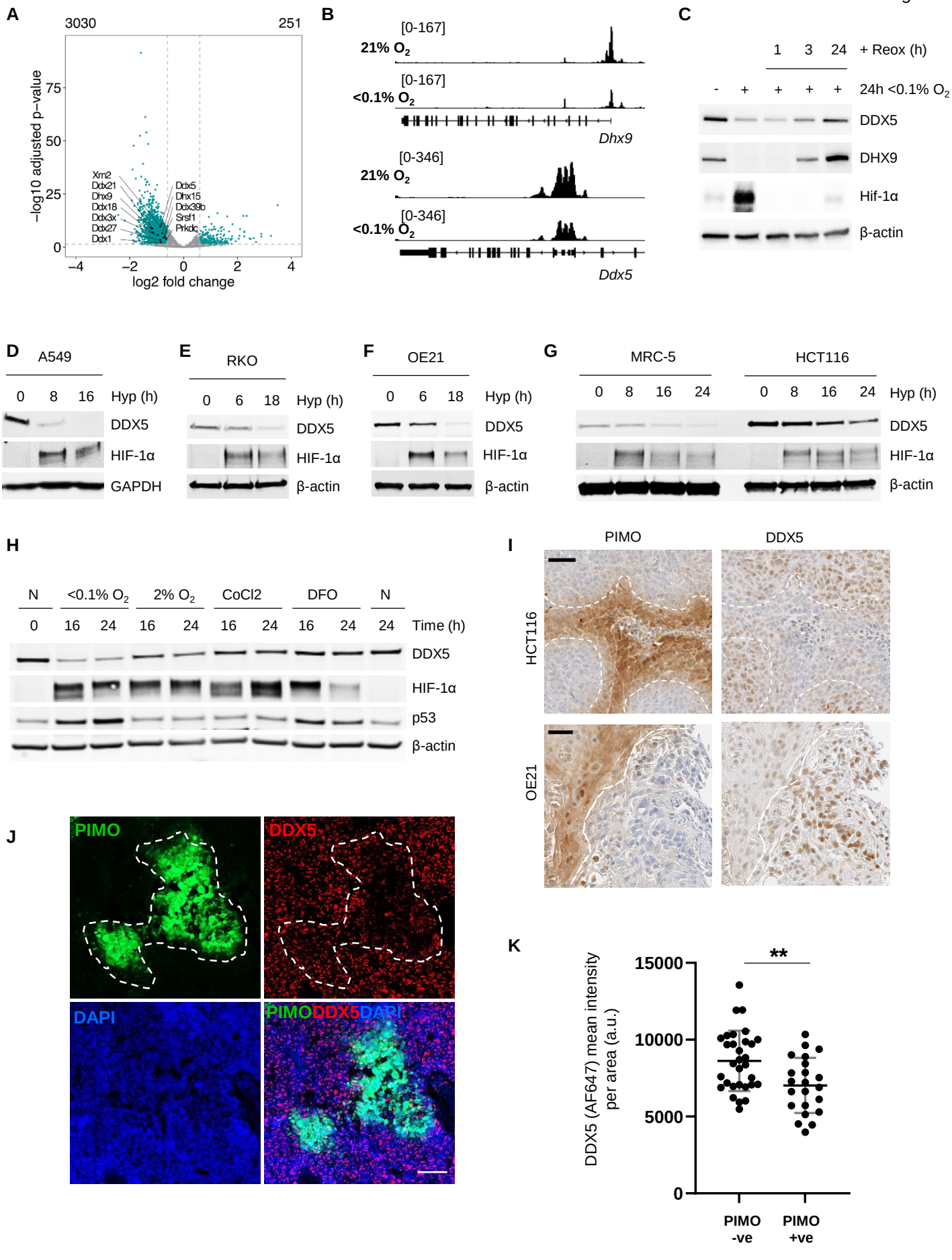
A
3030
251
−log10 adjusted p−value
log2 fold change
Xrn2
Ddx21
Dhx9
Ddx18
Ddx3x
Ddx27
Ddx1
Ddx5
Dhx15
Ddx39b
Srsf1
Prkdc
B
[0-167]
21% O2
[0-167]
<0.1% O2
Dhx9
[0-346]
21% O2
[0-346]
<0.1% O2
Ddx5
C
1 3 24 + Reox (h)
- + + + + 24h <0.1% O2
DDX5
DHX9
Hif-1α
β-actin
D
A549
0 8 16 Hyp (h)
DDX5
HIF-1α
GAPDH
E
RKO
0 6 18 Hyp (h)
DDX5
HIF-1α
β-actin
F
OE21
0 6 18 Hyp (h)
DDX5
HIF-1α
β-actin
G
MRC-5
HCT116
0 8 16 24 0 8 16 24 Hyp (h)
DDX5
HIF-1α
β-actin
H
N <0.1% O2 2% O2 CoCl2 DFO N
0 16 24 16 24 16 24 16 24 24 Time (h)
DDX5
HIF-1α
p53
β-actin
I
PIMO
DDX5
HCT116
OE21
J
PIMO
DDX5
DAPI
PIMODDX5DAPI
K
DDX5 (AF647) mean intensity per area (a.u.)
15000
10000
5000
0
**
PIMO -ve
PIMO +ve

A

Correlation of mRNA expression of DDX5 and hypoxia signature

TCGA datasets:	Spearman:	P:
Glioblastoma (n=166)	-0.31	<0.0001
Breast (n=1100)	-0.11	0.0002
Colorectal (n=382)	-0.05	0.3112
Bladder (n=408)	-0.12	0.0148
Lung adenocarcinoma (n=517)	-0.34	<0.0001
Lung squamous cell carcinoma (n=501)	-0.25	<0.0001

B

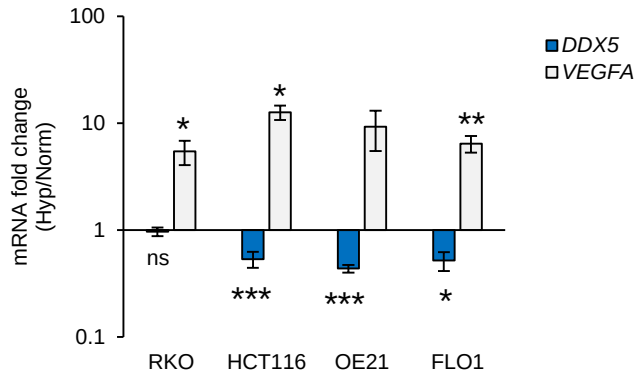

C

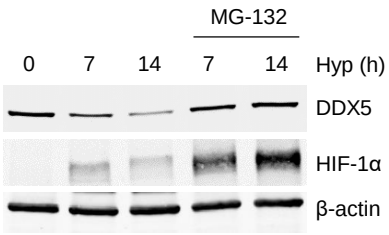

D

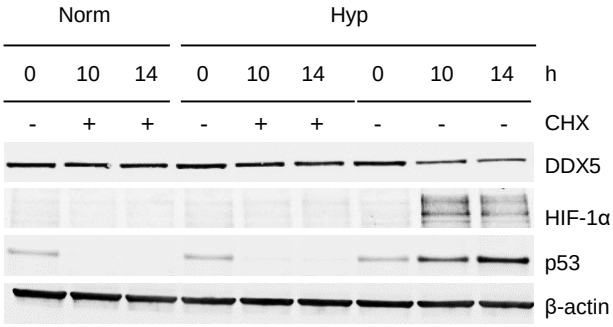

E

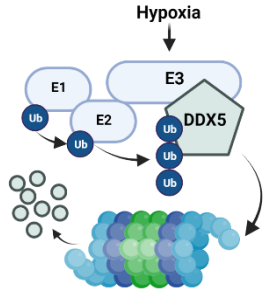

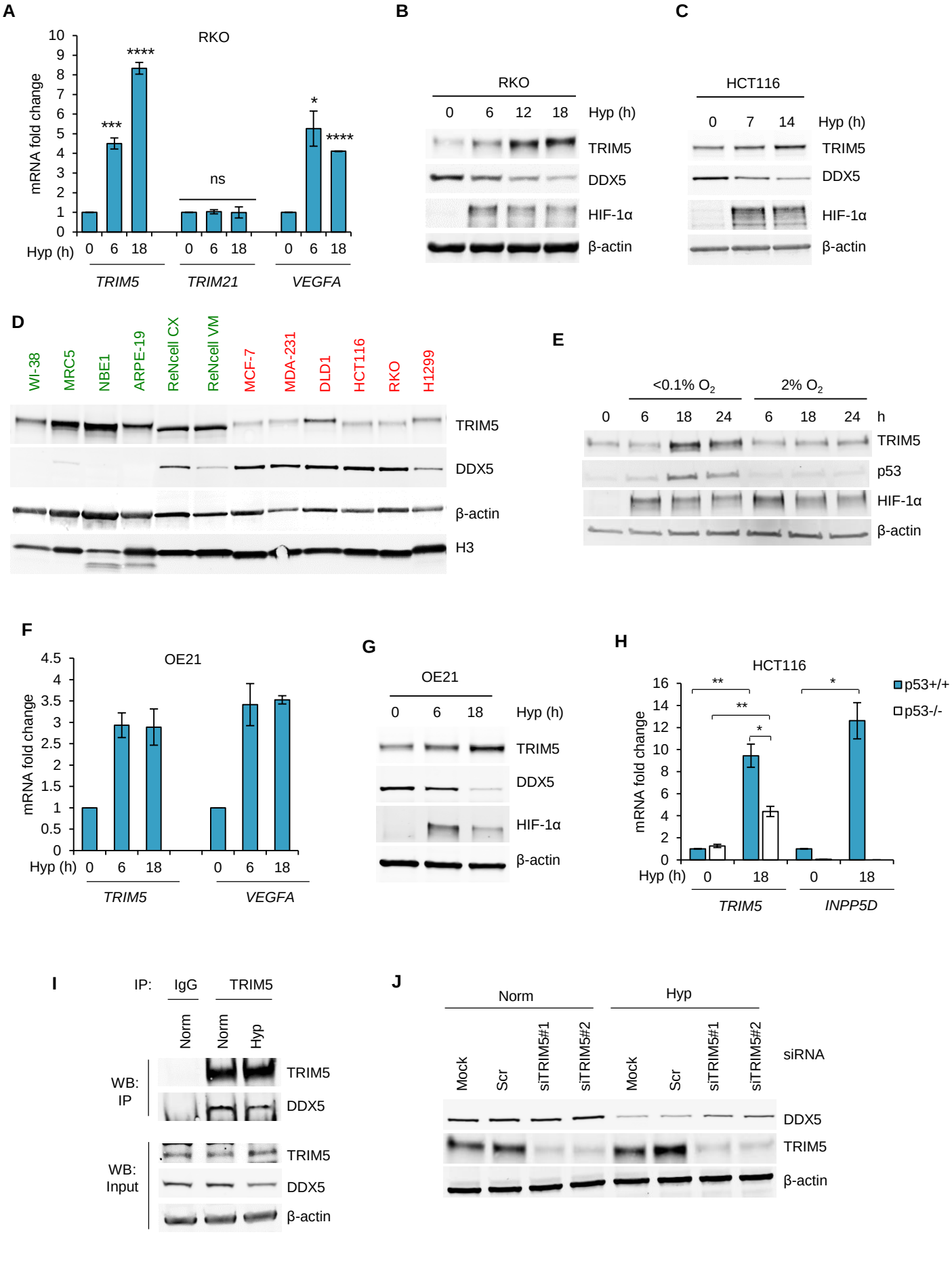
A
RKO
mRNA fold change
Hyp (h)
TRIM5
TRIM21
VEGFA
ns
B
RKO
Hyp (h)
TRIM5
DDX5
HIF-1α
β-actin
C
HCT116
Hyp (h)
TRIM5
DDX5
HIF-1α
β-actin
D
WI-38
MRC5
NBE1
ARPE-19
ReNcell CX
ReNcell VM
MCF-7
MDA-231
DLD1
HCT116
RKO
H1299
TRIM5
DDX5
β-actin
H3
E
<0.1% O2
2% O2
h
TRIM5
p53
HIF-1α
β-actin
F
OE21
mRNA fold change
Hyp (h)
TRIM5
VEGFA
G
OE21
Hyp (h)
TRIM5
DDX5
HIF-1α
β-actin
H
HCT116
mRNA fold change
p53+/+
p53-/-
Hyp (h)
TRIM5
INPP5D
I
IP:
IgG
TRIM5
Norm
Norm
Hyp
WB: IP
TRIM5
DDX5
WB: Input
TRIM5
DDX5
β-actin
J
Norm
Hyp
Mock
Scr
siTRIM5#1
siTRIM5#2
siRNA
DDX5
TRIM5
β-actin

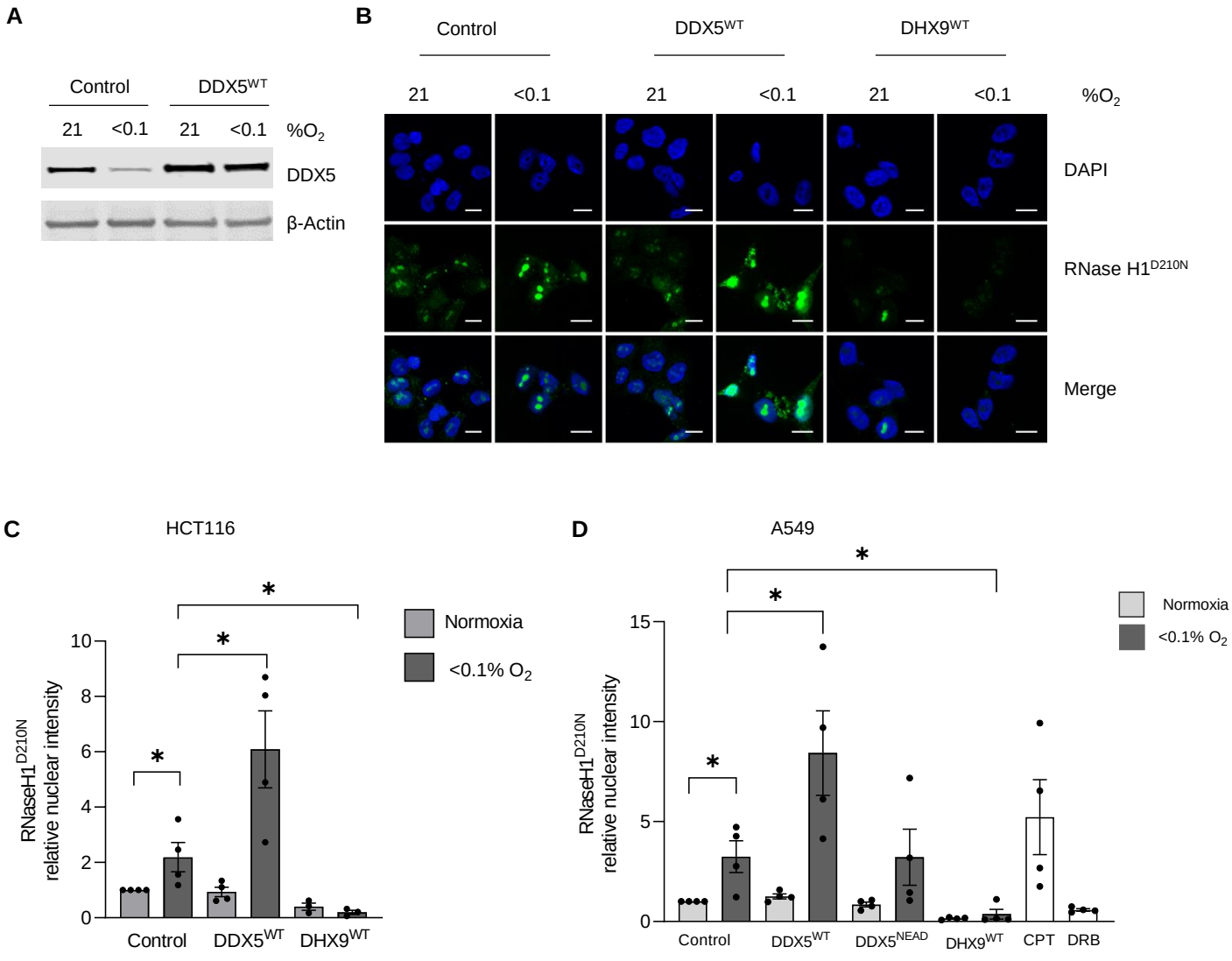
A
Control
DDX5WT
21
<0.1
21
<0.1
%O2
DDX5
β-Actin
B
Control
DDX5WT
DHX9WT
21
<0.1
21
<0.1
21
<0.1
%O2
DAPI
RNase H1D210N
Merge
C
HCT116
RNaseH1D210N relative nuclear intensity
Normoxia
<0.1% O2
Control
DDX5WT
DHX9WT
D
A549
RNaseH1D210N relative nuclear intensity
Normoxia
<0.1% O2
Control
DDX5WT
DDX5NEAD
DHX9WT
CPT
DRB